Chapter 8

Microstructure Analysis

8.1 Introduction

The present chapter deals with the microstructural study for the low cycle fatigue analysis. The microstractural study is based on XRD analysis, optical micrography and scanning electron micrography. Crystallite sizes are determined for each cases of low cycle fatigue analysis presented earlier. Variation of crystallite size with the respect to heat treatment temperature and soaking time are presented. Optical micrographic pictures are presented for as received AA6063 alloy and AA6063/SiCp MMC cases. Scanning electron micrography are presented for as received AA6063 alloy, heat treated AA6063 alloy at different temperatures, heat treated AA6063 alloy at same temperature with different soaking times and AA6063/SiCp MMC.

8.2 X-RD Test

8.2.1 As Received

The crystal structure in the sample is investigated thourough XRD analysis. The intensities and the angular position of the Bragg peaks in the diffraction pattern are shown in Fig. 8.1.

The XRD spectra of the sample clearly shows the major 2θ peaks of aluminium. The diameters of the crystallize size and intensity of Bragg peaks at different 2θ angles are obtained from experimental results without loading as shown in Table 8.1, and

compared with the results given in JCPDF (Joint Committee for Powder Diffraction Standards) File No. 851327 for aluminium Cubic system .

The micro structural information is predicted from broadening of the Bragg peaks. The total broadening is due to instrumental broadening and broadening due to average domain size and the lattice micro strains. The crystal structure in the sample is investigated thourough XRD analysis, the crystal structure is predicted from the intensities and the angular position of the Bragg peaks in the diffraction pattern as shown in Fig. 8.1.

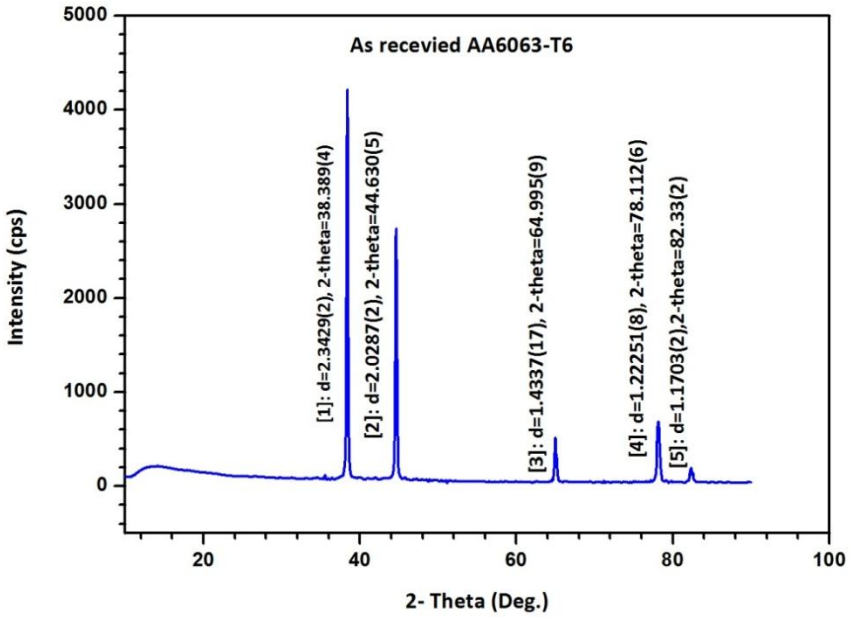

Fig. 8.1 X-RD Pattern for as received AA6063-T6 alloy at room temperature

X-RD test was also done for the samples which were tested for low cycle fatigue at different loads viz. 4.5Kg (elastic zone) 6.9Kg (yield point) and 7.839Kg and 8.55Kg (plastic zone). The intensities and crystallite size for these cases also are presented in Table 8.1. Also the Crystallite size and diameter for as-received condition AA6063-T6 at different loads are reported in Table 8.2.

Table 8.1 JCPDF data for intensity and crystallites for as-received AA6063-T6 samples LCF tested with different loading and untested (no load)

S.NO.	H k l Miller indices of the Bragg reflections	No Load (untested)				With Loading (LCF tested)							
		d(A)		Intensity		d(A)				Intensity			
		JCPDF	Expt.	JCPDF	Expt.	83.8N	72.5N	67.1N	44.1N	83.8N	72.5N	67.1N	44.1N
1	1 1 1	2.3379	2.3428	999	716.41	5.7729	6.1921	5.8169	5.7480	65.43	272.2	116.71	50.75
2	2 0 0	2.0247	2.0286	455	509.44	2.3430	2.344	3.1229	2.3446	1947.8	136.48	17.07	219.9
3	2 2 0	1.4316	1.4337	233	111.73	2.0295	2.0285	2.3440	2.0298	1548.8	1656.18	86.65	1547.2
4	3 1 1	1.2209	1.2225	228	211.58	1.2221	1.2222	2.2486	1.2225	292.95	386.53	23.72	145.36
5	2 2 2	1.689	1.17027	63	50.27	1.1700	1.1700	2.0285	1.1700	357.58	99.19	4218.0	41.34

Table 8.2 Crystallite size and diameter for as-received condition AA6063-T6 LCF tested at different loads

Load (Kg)	Diameter of sample at fracture, d_f (mm)	Crystallite size (nm)	Number of cycles to failure $2N_f$
--	--	91.834	Untested
4.5	6.2	128.24	141300
6.9	7	166.84	63300
7.38	6.6	122.922	60150
8.55	6.94	152.989	7080

Figure 8.2 shows that crystallite size increase with increase in load as applied during LCF test. The crystallite size increases with increase in number of cycles of failure as illustrate in Fig. 8.3. Figure 8.4 demonstrates the variation of diameter of sample at fracture with number of cycles to failure. It is observed that the diameter of sample at fracture has a decreasing tendency with number of cycles to failure.

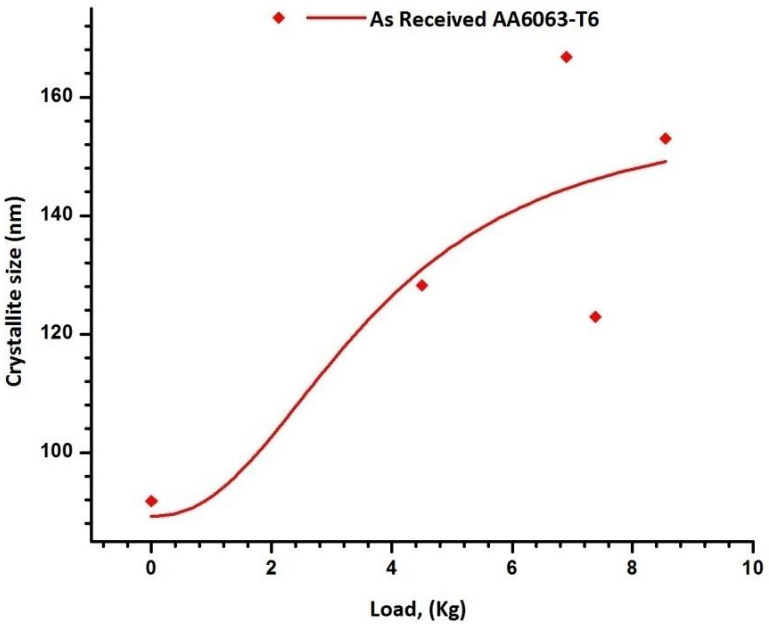

Fig. 8.2 Variation of crystallite size with load of LCF test

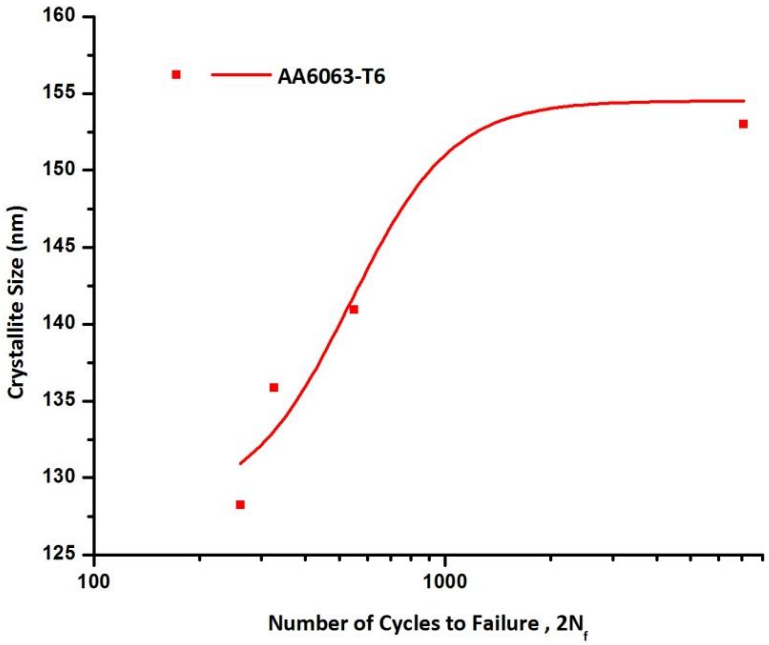

Fig. 8.3 Variation of crystallite size with the number of cycles to failure

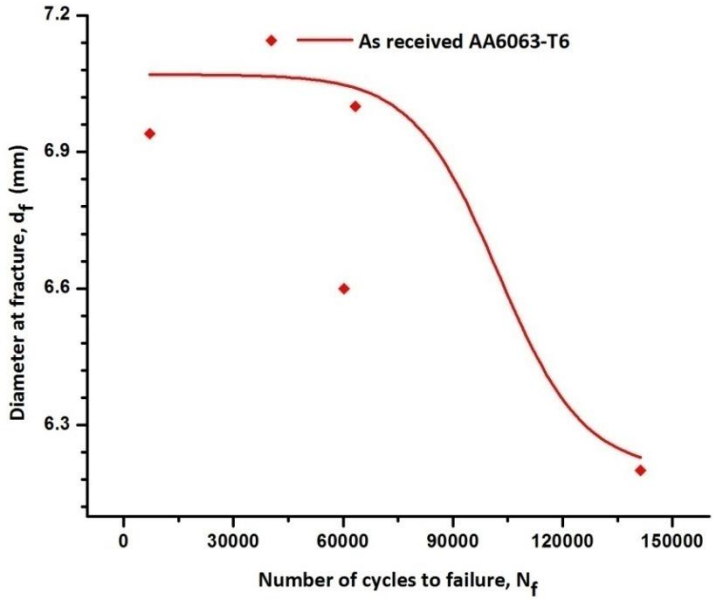

Fig. 8.4 Variation of diameter of sample at fracture with the number of cycles to failure

8.2.2 AA6063 at different temperatures

Figures 8.5 and 8.6 show XRD patterns for AA6063 samples heat treated at 200℃ and 350℃, respectively and soaked for same time of 2 hours.

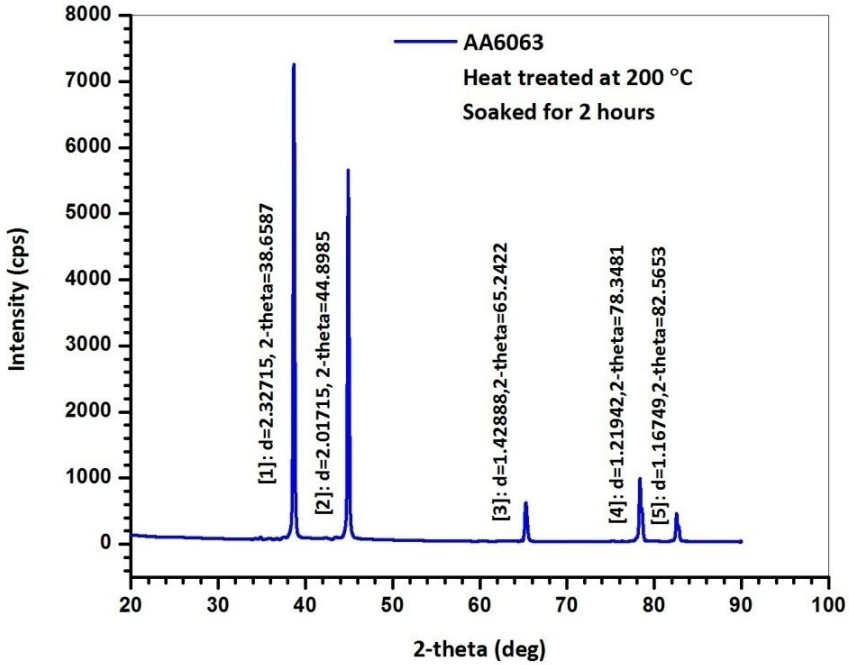

Fig. 8.5 X-RD pattern for AA6063 heat treated at 200℃ and soaked for 2 hours

Table 8.3 shows data of crystallite size, diameter of sample at fracture and number of cycles to failure for as received AA6063 and two heat treatment cases.

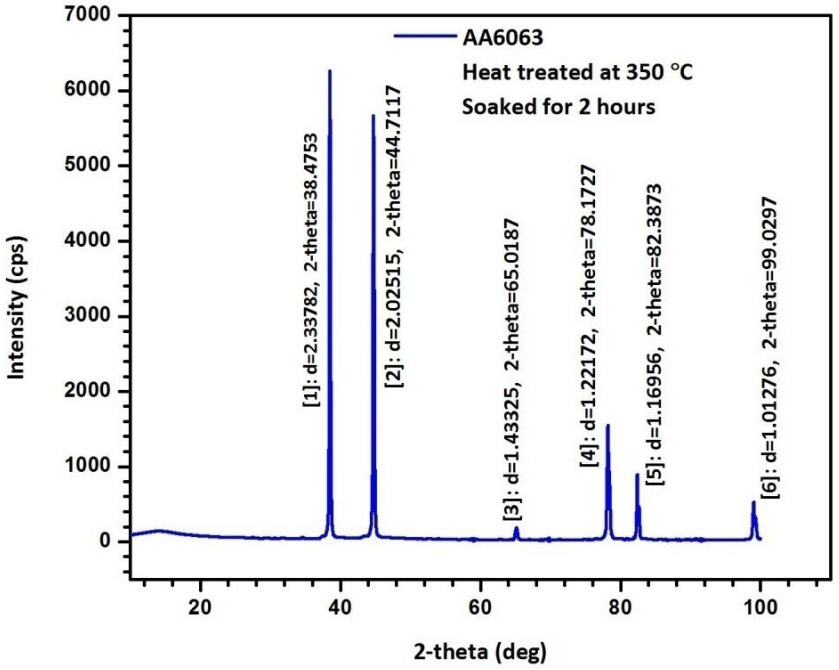

Fig. 8.6 X-RD pattern for AA6063 heat treated at 350℃ and soaked for 2 hours

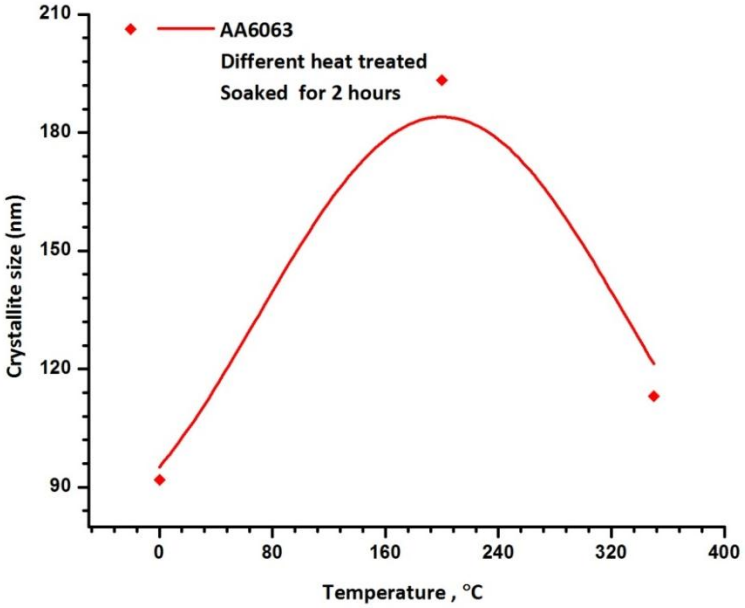

Fig. 8.7 Variation of crystallite size with different heat treatment temperature for same soaking time of 2 hours

Figure 8.7 demonstrates variation of crystallite size with heat treatment temperature for same soaking time of 2 hours. Variation of diameter of sample at fracture with the different heat treatment temperature at same soaking time of 2 hours show in Fig. 8.8 . The variation of diameter of sample at fracture with heat treatment temperature is demonstrated in Fig. 8.9. It is observed that the diameter of sample at fracture increases with increase in number of cycles to failure.

Table 8.3 Crystallite size and diameter of sample at fracture data for AA6063 with different heat treatment temperature for same soaking time of 2 hours

AA 6063 Conditions	Crystallite size nm	Diameter of sample at fracture (mm)	Number of cycles of failure, N_f
As received	152.989	6.94	7080
200℃-2hour	193.344	6.81	792
350℃-2hour	113.07	6.63	613

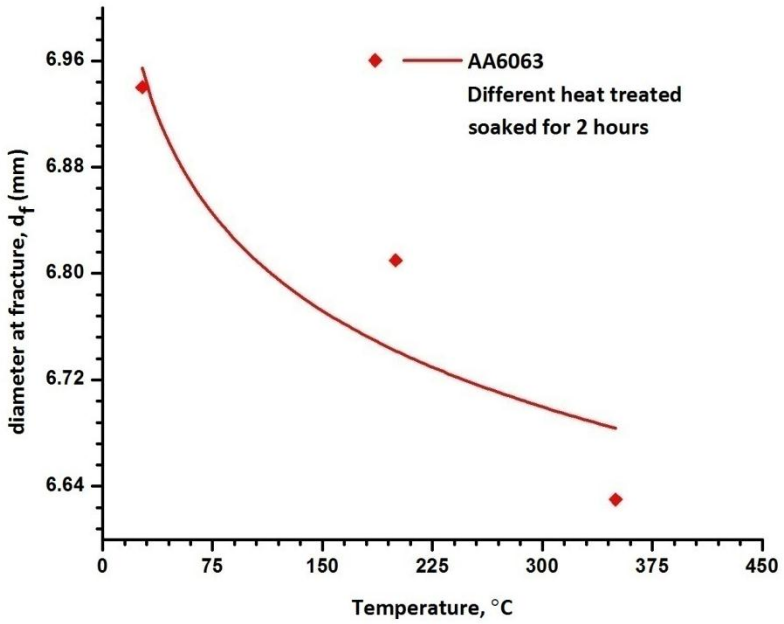

Fig. 8.8 Variation of diameter of sample at fracture with the different treat temperature and same soaking time of 2 hours

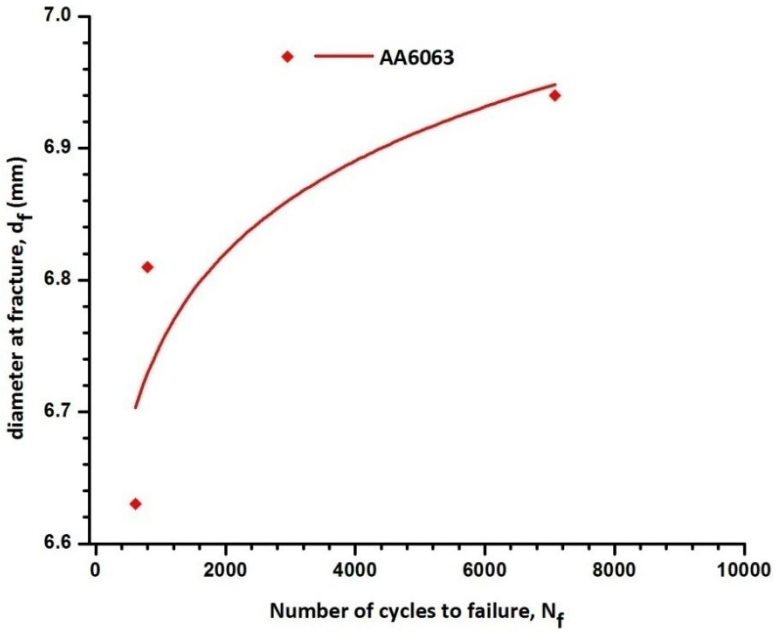

Fig. 8.9 Variation of diameter of sample at fracture with the number of cycles to failure for same soaking time of 2 hours

8.2.3 AA6063 at different soaking times

Figure 8.10 to 8.12 show patterns for AA6063 samples heat treated at 350℃ and soaked for 4 hours, 6 hours and 8 hours, respectively. Table 8.4 shows data of crystallite size, diameter of sample at fracture and numbers of cycles of failure for as received AA6063 and four heat treatment cases where heat treatment temperature is 350℃ and soaking times are 2 hours, 4 hours, 6 hours and 8 hours. The variation of diameter at fracture of the sample with different soaking time of heat treatment at same heat treatment temperature of 350℃ illustrated in Fig. 8.13. Figure 8.14 demonstrates the variation of crystallite size with soaking time of heat treatment at same heat treatment temperature of 350℃. Variation of diameter of sample at fracture with soaking time of heat treatment at same heat treatment temperature of 350℃ is illustrated in Fig. 8.15. It is

observed that the diameter of sample at fracture has a decreasing till certain number of cycles after that increases with number of cycles to failure.

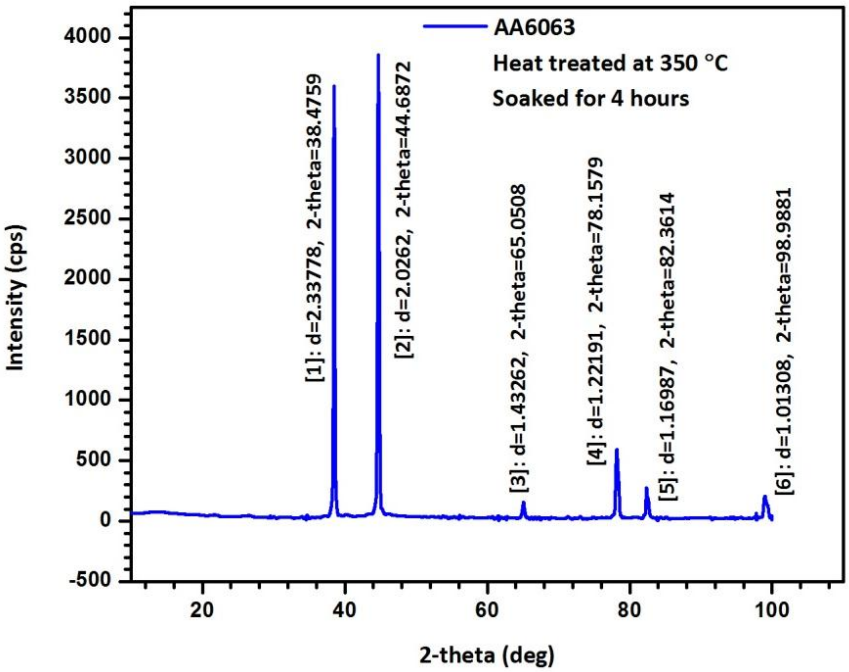

Fig. 8.10 X-RD Pattern for AA6063 heat treated at 350℃ and soaked for 4 hours

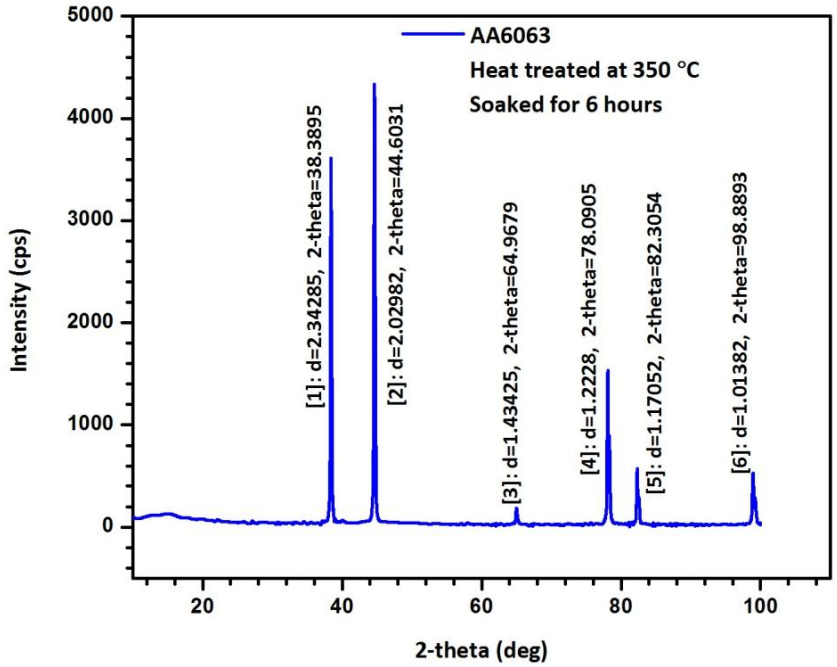

Fig. 8.11 X-RD Pattern for AA6063 heat treated at 350℃ and soaked for 6 hours

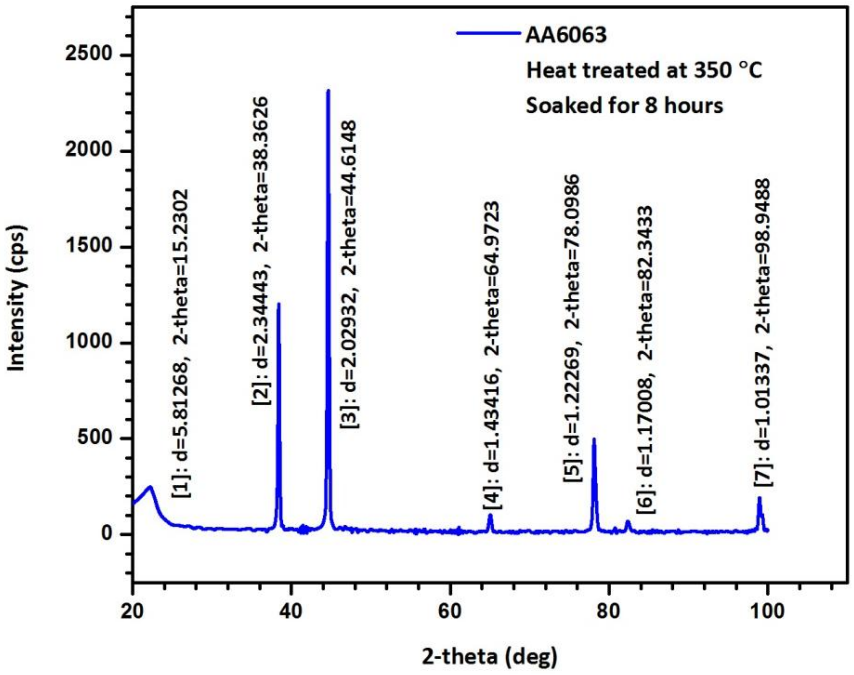

Fig. 8.12 X-RD Pattern for AA6063 heat treated at 350℃ and soaked for 8 hours

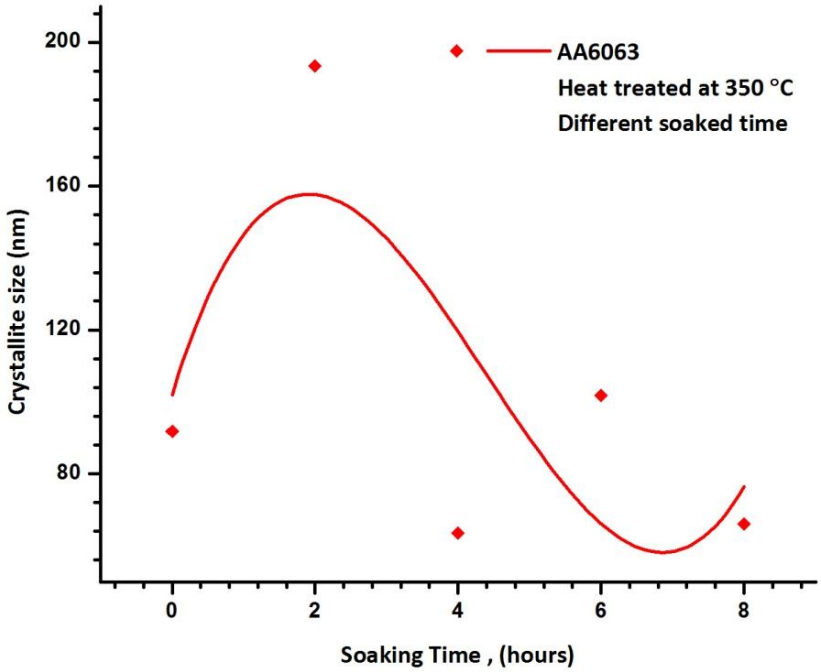

Fig. 8.13 Variation of crystallite size with different soaking time for same heat treatment temperature of 350℃

Table 8.4 Crystallite size and diameter of sample at fracture data for AA6063 with different soaking time for same heat treatment temperature of 350℃

Heat treatment Temp. 350℃ with soaking time (hour)	Crystallite size (nm)	Diameter of sample at fracture (mm)	Number of cycles of failure, N_f
As received	91.834	6.94	7080
2	113.07	6.63	613
4	63.47	6.5	1012
6	101.832	6.6	819
8	66.149	6.99	211

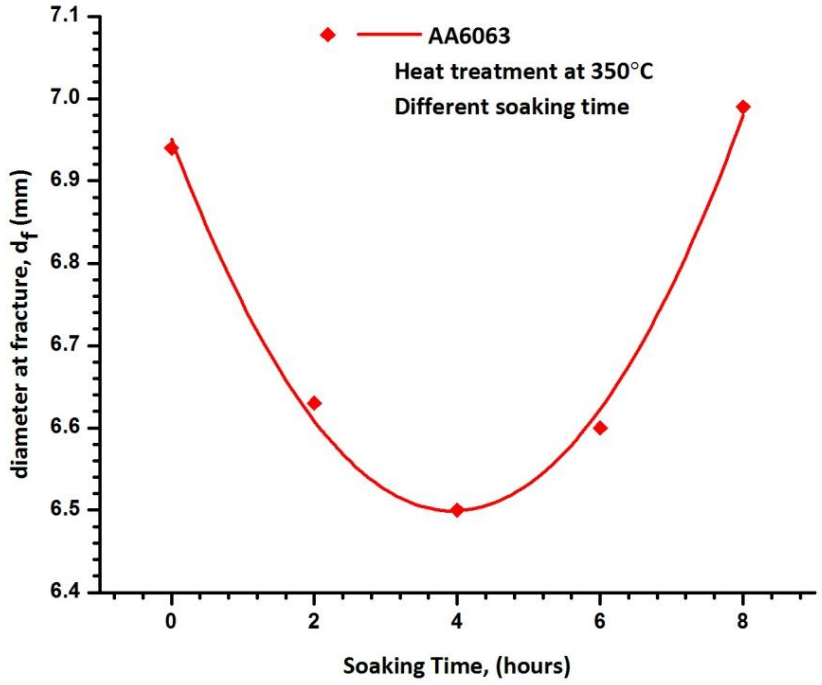

Fig. 8.14 Variation of diameter of sample at fracture with different soaking time for same heat treatment temperature of 350℃

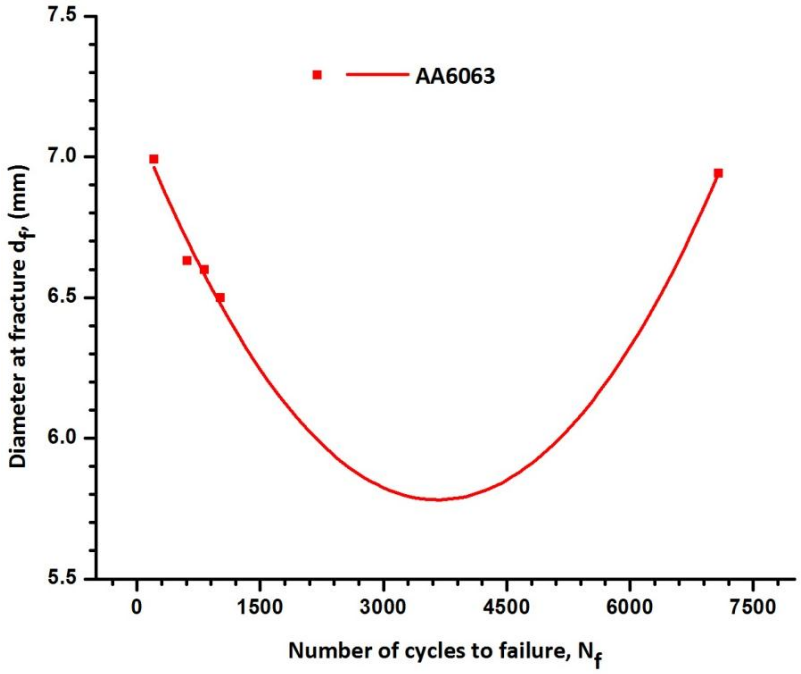

Fig. 8.15 Variation of diameter of sample at fracture with the number of cycles to failure for same heat treatment temperature of 350℃

8.2.4 AA6063/SiCp MMC

Figure 8.16 and 8.17 show XRD patterns for AA6063/SiCp (2% V_f) MMC and AA6063/SiCp (8% V_f) MMCs, respectively at room temperature condition. Table 8.5 shows data of crystallite size, diameter of sample at fracture and numbers of cycles of failure for as received AA6063, AA6063/SiCp (2% V_f) MMC and AA6063/SiCp (8% V_f) MMCs. The variation of crystallite size with different volume fraction of reinforcement particle of MMC illustrate in Fig. 8.18. It is observed that the crystallite size has a increase till certain volume fraction after that decrease.

Figure 8.19 illustrates variation of crystallite size with reinforcement volume fraction of MMC. The variation of diameter of sample at fracture with reinforcement volume fraction of MMC is demonstrated in Fig. 8.20. It is observed that the diameter of sample at fracture has a decreasing tendency with number of cycles to failure.

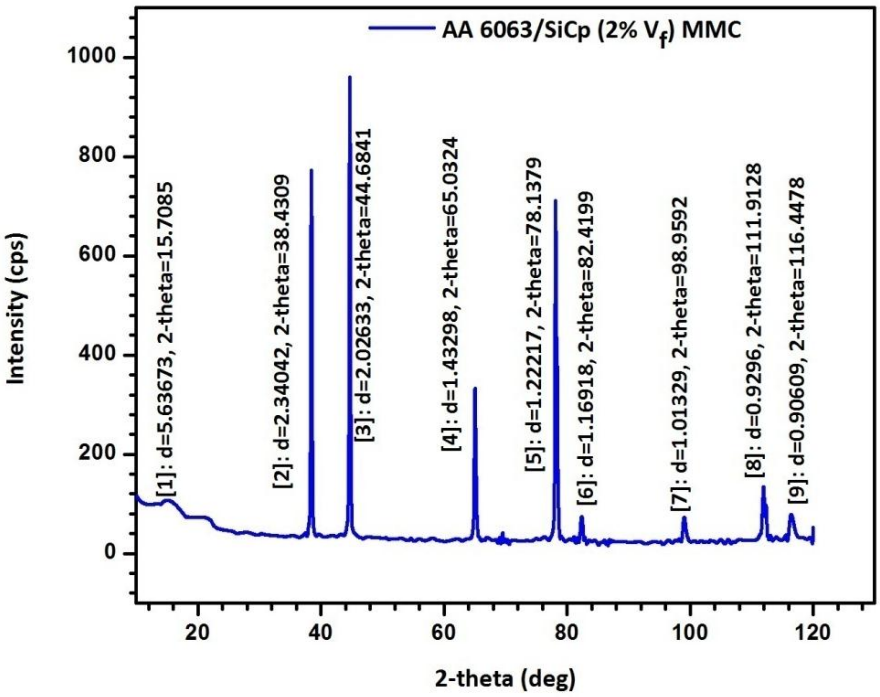

Fig. 8.16 X-RD pattern for AA6063/SiCp (2% V_f) MMC

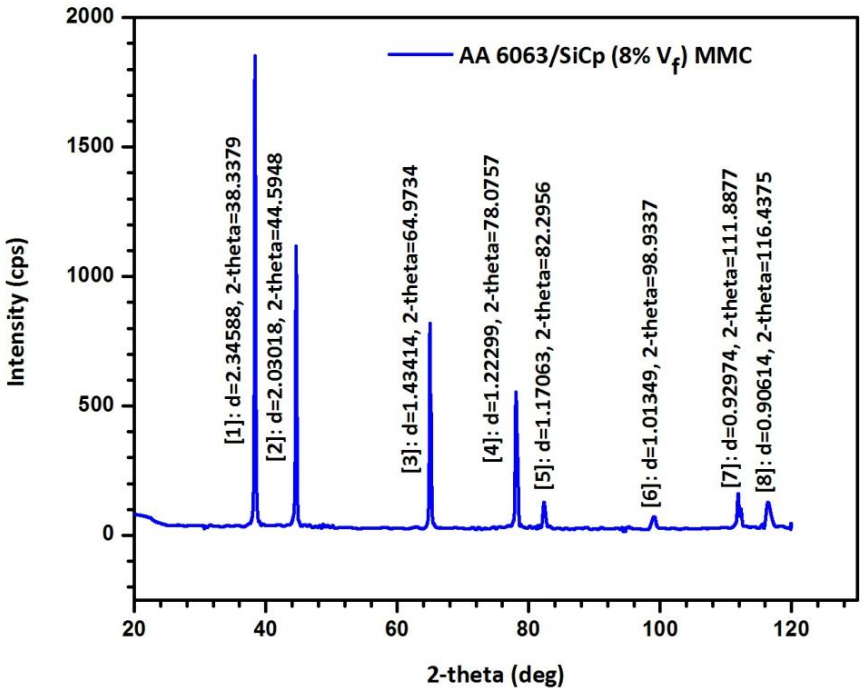

Fig. 8.17 X-RD pattern for AA6063/SiCp (2% V_f) MMC

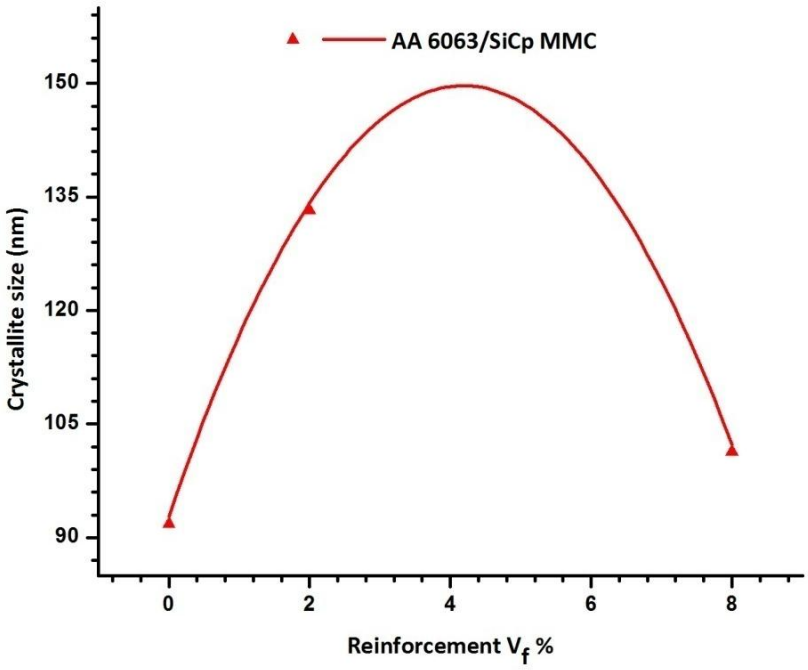

Fig. 8.18 Variation of crystallite size with different volume fraction of reinforcement particle of MMC

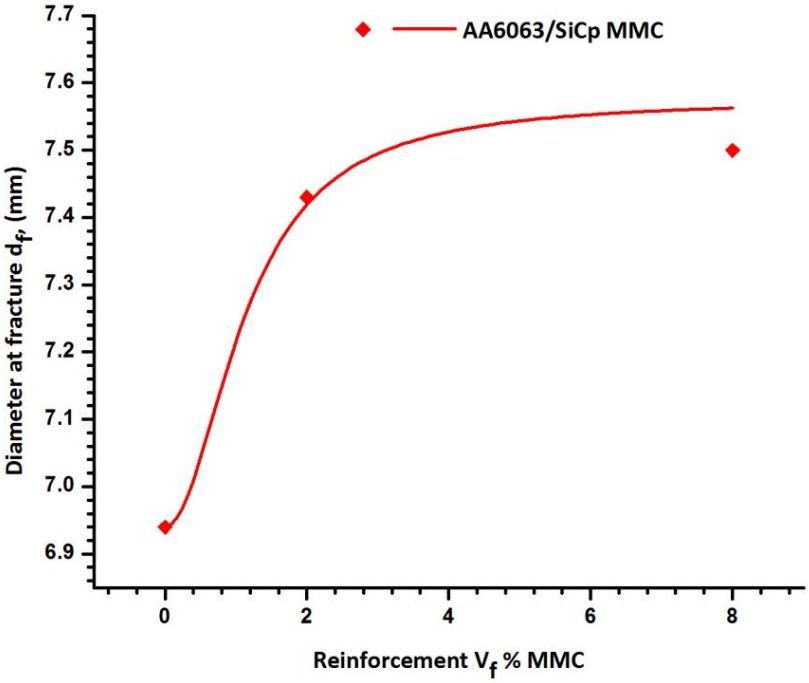

Fig. 8.19 Variation of diameter of sample at fracture with reinforcement particle of AA6063/SiCp V_f MMC

Table 8.5 Crystallite size and diameter of sample at fracture data for AA6063/SiCp MMC

Samples	Crystallite size nm	Diameter of sample at fracture (mm)	Number of cycles of failure, N_f
As received AA6063	91.834	6.94	7080
AA6063/SiCp (2% V_f)	133.26	7.43	311
AA6063/SiCp (8% V_f)	101.37	7.5	310

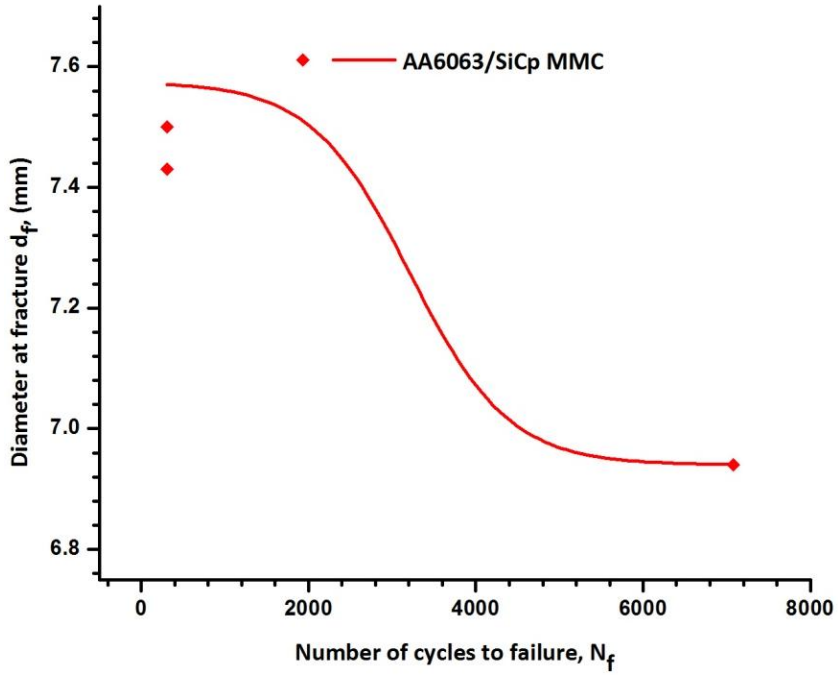

Fig. 8.20 Variation of diameter of sample at fracture with the number of cycles to failure of reinforcement particle of MMC

8.3 Optical Micrograph

8.3.1 As received AA6063 –T6

To study the microstructure features Optical Micrograph pictures were taken with different magnification before and after fatigue test as shown in Fig. 8.21. It is observed that Silicon (Si) and Magnesium (Mg) particles are observed in Fig. 8.21 (a) at 50x magnification there is no visible crack in the micrograph before test.

However after test cracks are generated at the grain boundaries as observed from Figure 8.21(b) at 50x magnification and Fig. 8.21 (d) at 100x magnification. Slip-Band dislocation are also observed in these figures.

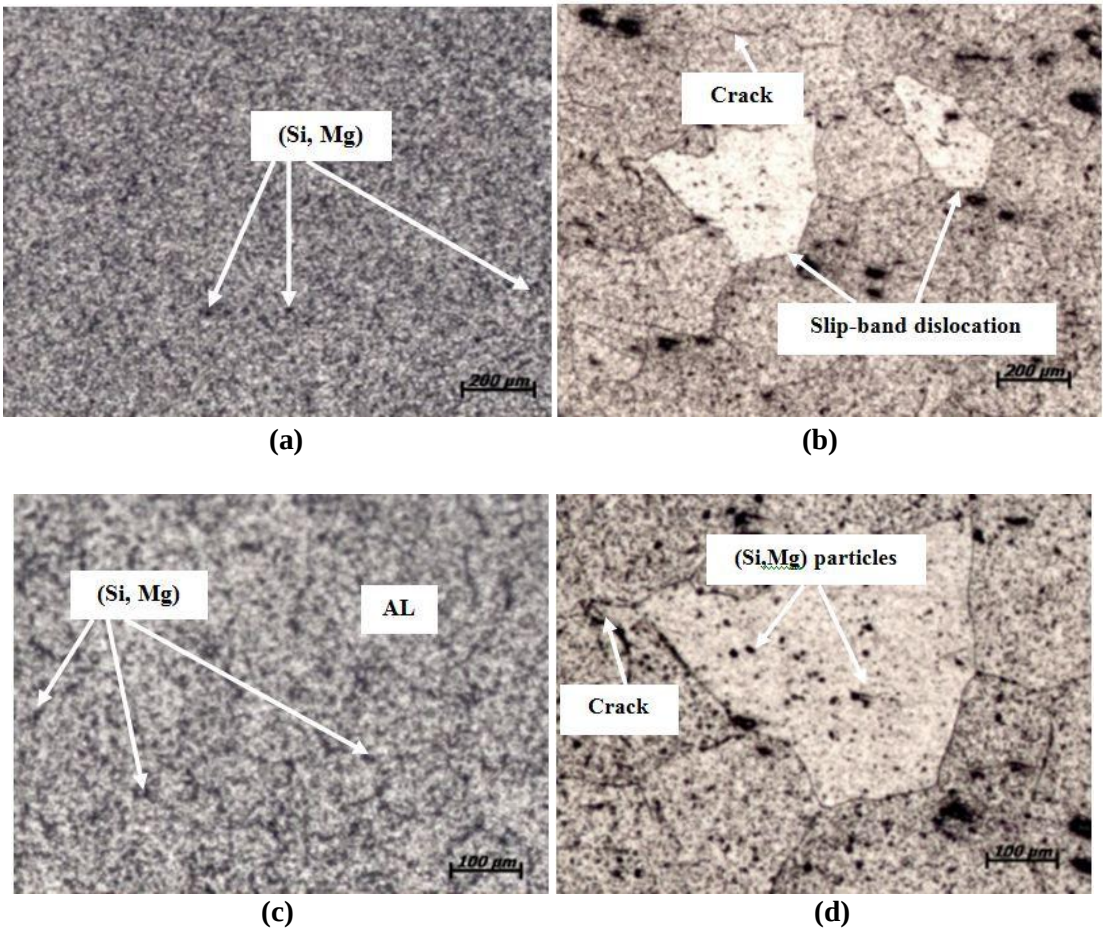

Fig. 8.21 Optical micrograph for AA6063 as received samples
(a) before the test at 50x magnification, (b) after the test at 50x magnification
(c) before the test at 100x magnification, (d) after the test at 100x magnification

8.3.2 AA6063/SiCp MMC

Figure 8.22 show optical micrograph pictures of AA6063/SiCp MMC for 2% V_f and 8% V_f cases at 50x,100x and 200x magnification before LCF test. The micrographs clearly show the SiCp particales and more densities are observed for 8% V_f MMC than 2% V_f MMC.

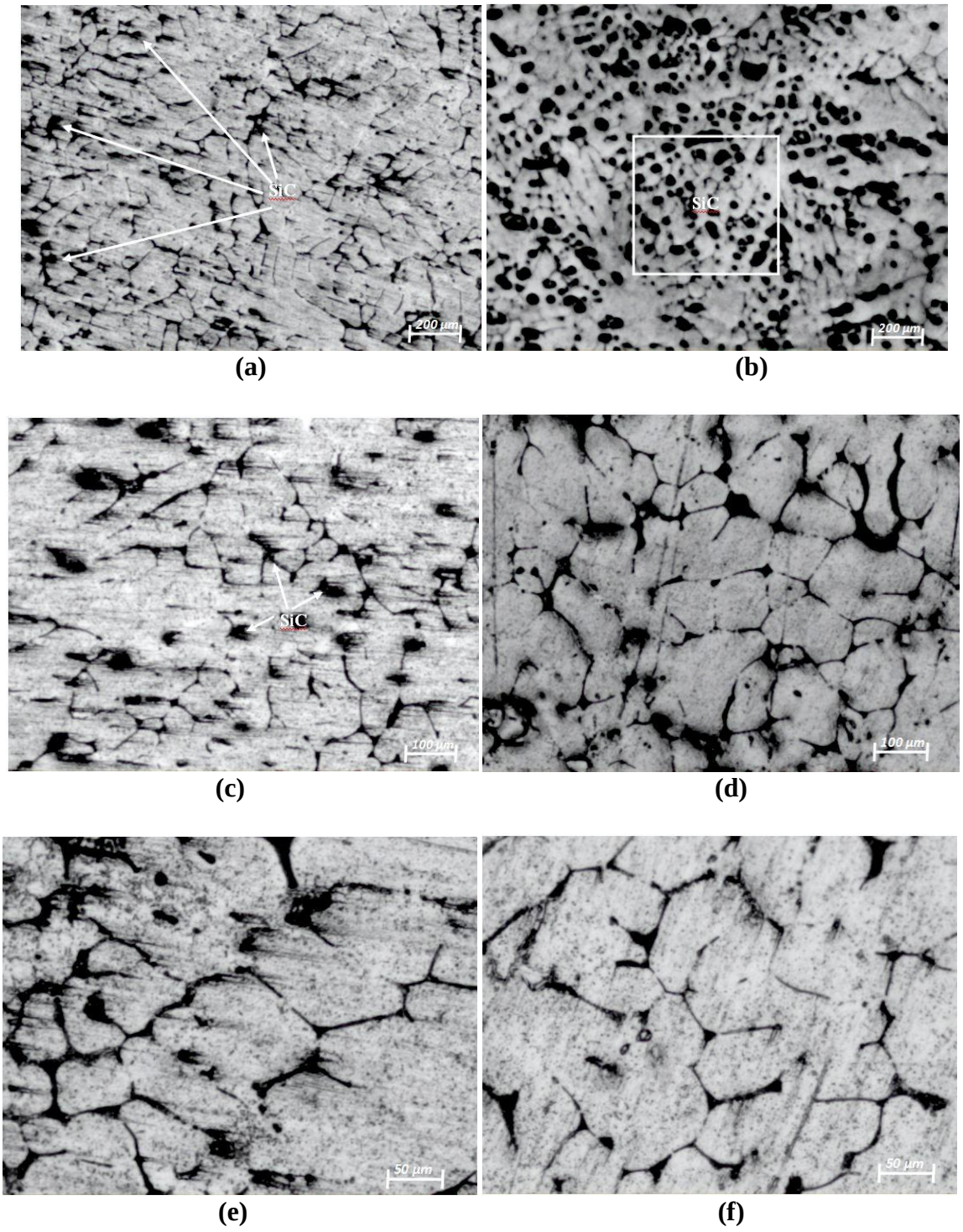

Fig. 8.22 Microstructure of the AA6063/SiCp MMC

(a) 2% V_f 50x magnification, (b) 8% V_f 50x magnification

(c) 2% V_f 100x magnification, (d) 8% V_f 100x magnification

(e) 2% V_f 200x magnification, (f) 8% V_f 200x magnification

8.4 SEM Micrograph

8.4.1 As received AA6063 –T6

Figure 8.23 illustrates SEM images at high magnification before the test. The location c has a relatively coarse grain structure.

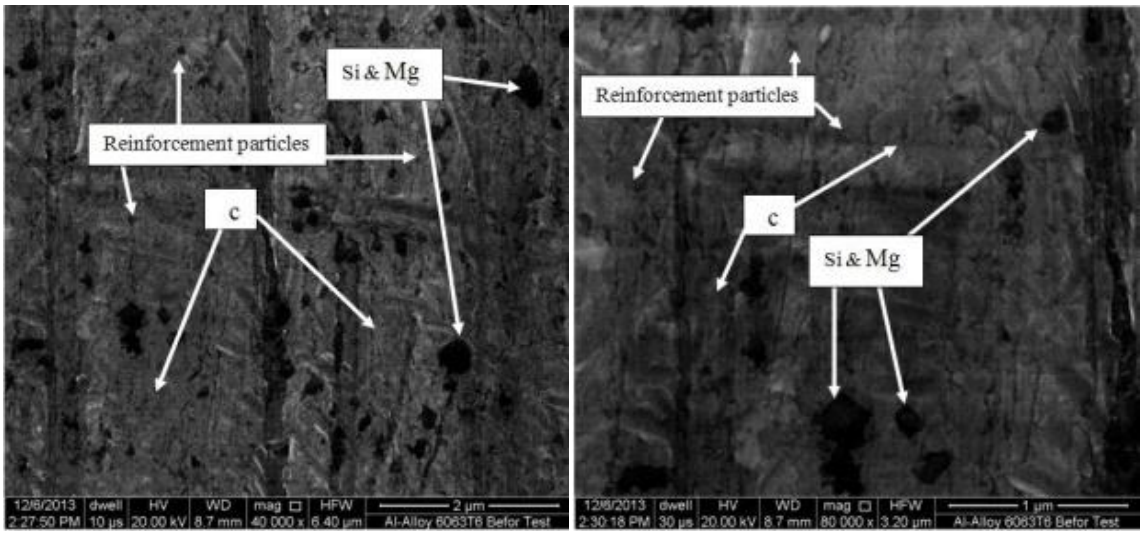

(a) **(b)**

Fig. 8.23 SEM picture before the test at:

(a) 40000x magnification, (b) 80000x magnification

Figure 8.24 shows SEM pictures after LCF test for as received AA6063 samples at 40x, 47x, 150x, 160x, 300x, 600x magnifications.

Also of interest is the shape of the overload zone. The fact that it is elongated overload zone indicates some plane bending loads were present. More than one points of origin are obseved where the crack actually started, which may be the result of either high stress or high stress concentrations.

A view in Fig. 8.24(f) shows multiple ratchet marks separating the failure origins. It can be noted that the origins are not on the same plane and that the ratchet marks are in effect boundaries between the fracture planes. In fact, there is yet another origin on the

other side of the failure face. It can be observed from Fig. 8.24(e)**,** the particle cracking and cleavage between Si and matrix material became more evident.

There were a few observations of pull out of particles from the aluminium matrix, which indicates quite a good interfacial bonding. From the figure the plateau etching can be observed which shows the fracture and microstructure features.

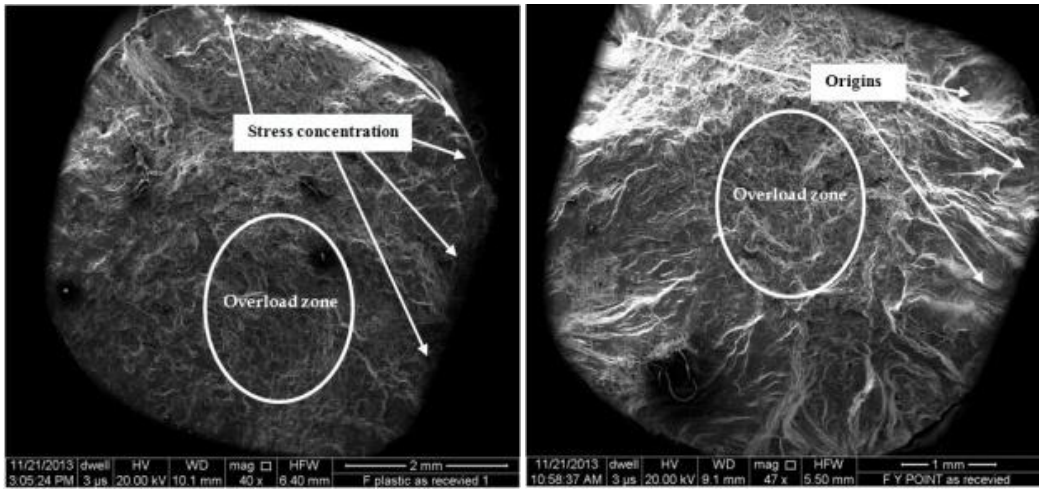

(a) **(b)**

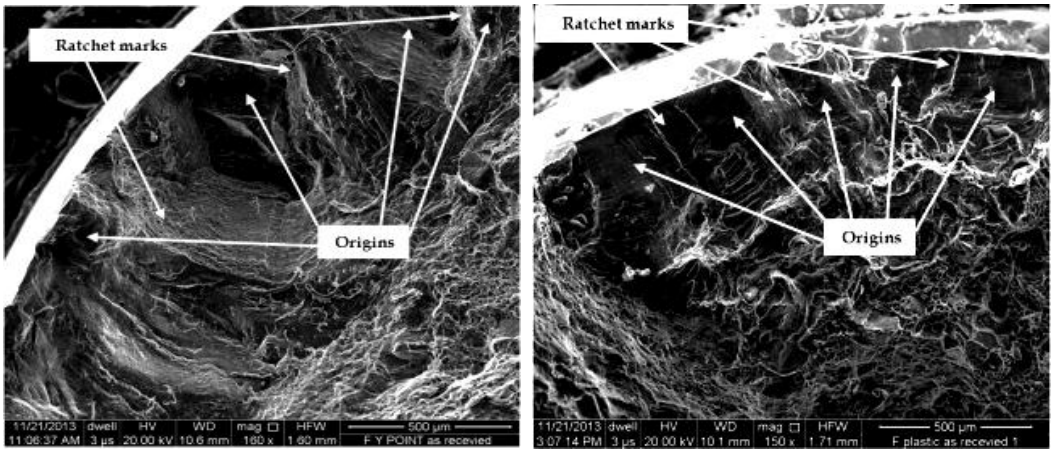

(c) **(d)**

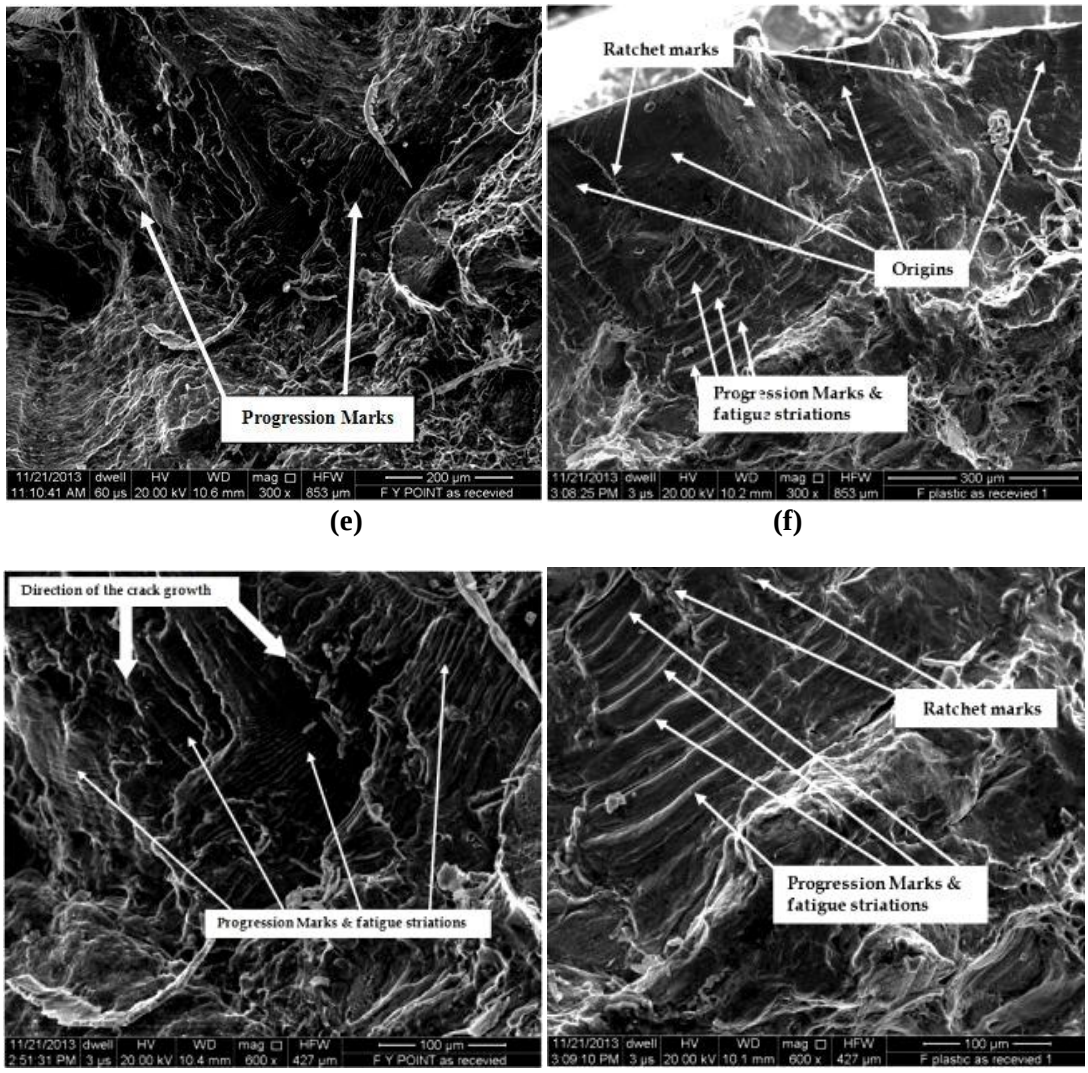

(e) **(f)**

(g) **(h)**

Fig. 8.24 SEM pictures after the LCF test for AA6063 as received at:

(a) 40x magnification (b) 47x magnification

(c) 160x magnification (d) 150x magnification

(e) 300x magnification (f) 300x magnification

(g) 600x magnification (h) 600x magnification

Figures 8.24g and 8.24h show progression of fatigue crack which look like a river on physical map, which show the direction of progression of the fatigue crack. In same time at high magnification we can see the progression Marks (beach marks), and these marks

will tell exactly how the crack face has progressed across the test piece and are only present in fractures. Ductile striations with large, regular size and spacing can also be observed**.** It can also be observed from Fig. 8.24(g, h) that there are regular fatigue striations due to regular loading cycle.

8.4.2 AA6063 at different heat treatment temperatures

The fracture surface of the tensile tested samples was examined using scanning electron microscope (SEM). Ductile fracture was observed in all conditions, but at high heat treatment temperature ductility and deformations was observed very high in comparison to low heat treatment temperature conditions. It may be seen from these fractographs that dimple morphology was predominant at room temperature as well as at high heat treatment temperatures. Further, the dimple size was found to increase with temperatures, as can be observed from Fig. 8.25.

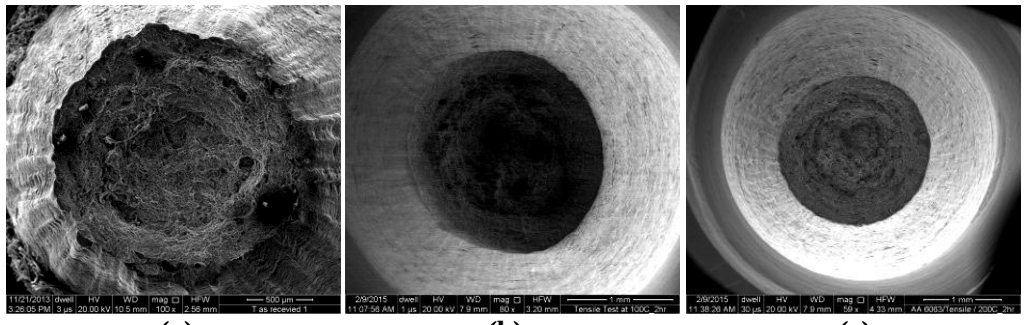

(a) **(b)** **(c)**

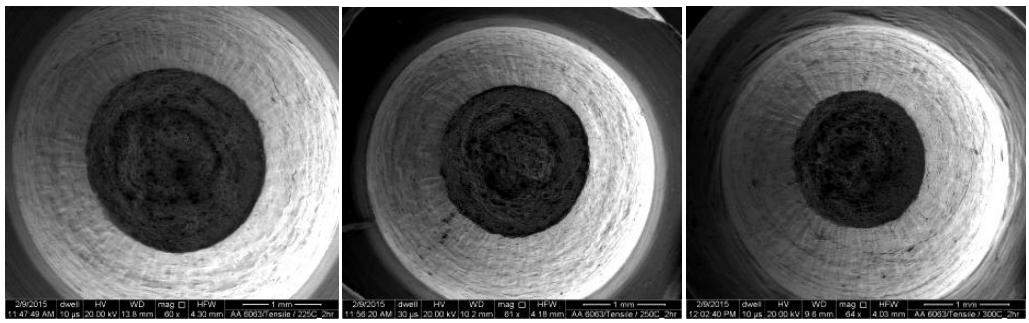

(d) **(e)** **(f)**

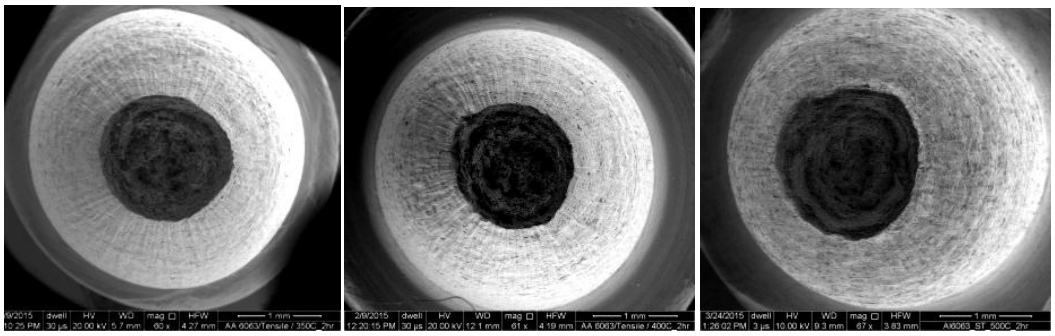

(g) (h) (i)

Fig. 8.25 SEM over view pictures for the tensile surface fracture test at different heat treatment temperatures:
(a) as received, (b) 100°C , (c) 200°C, (d) 225°C, (e) 250°C , (f) 300°C (g) 350°C, (h) 400°C , (i) 500°C

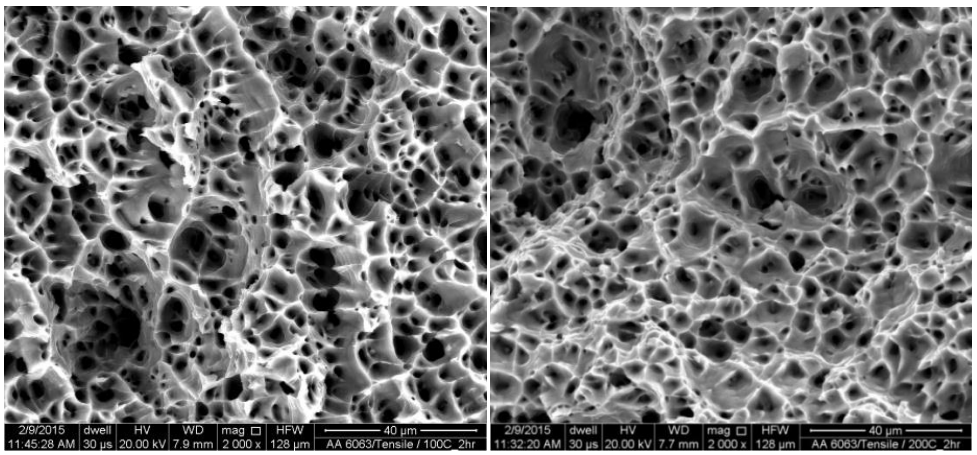

(a) (b)

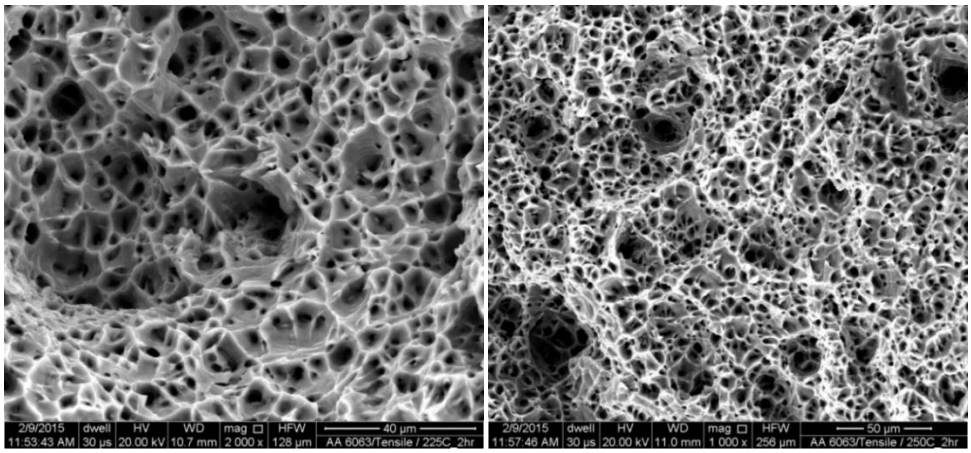

(c) (d)

Fig. 8.26 Honeycomb structure (dimples) on the surface of fractures of tensile specimens of AA6063 at :

(a) 100°*C* , (b) 200°*C*, (c) 225°*C*, (d) 250°C

The plateau etching is observed in SEM pictures of tensile tested samples given in Figure 8.26 and 8.27. These micrographs depict the honeycomb structure and help to reproduce its formation, fractured crystallites. The second-phase precipitates are also visible at the bottom of the larger dimples in these micrograph. Plastic or ductile fracture is characterized by arrangements of dimples which form a kind of honeycomb structure. The dimple size must depend on the type, shape, size, distribution, and number of inclusions and precipitates, grain size and plastic properties of the material.

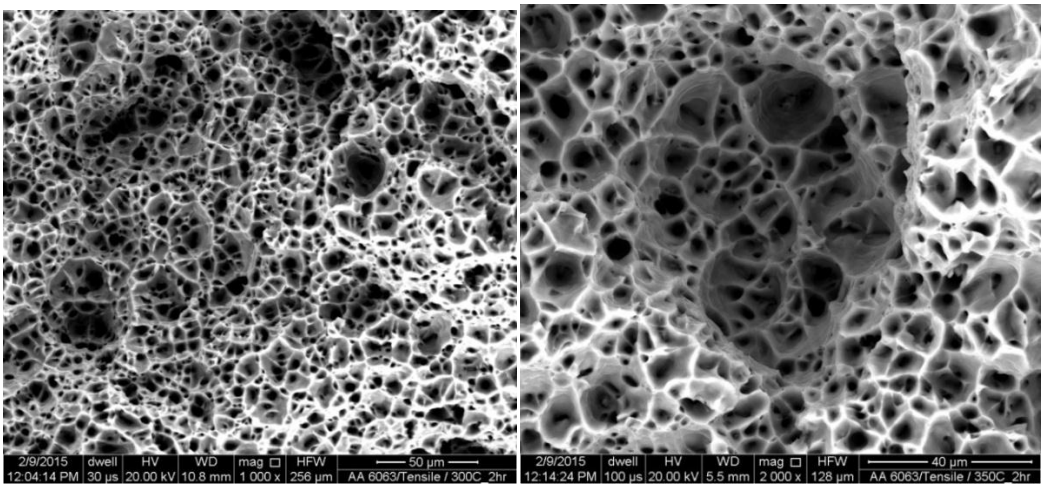

(a) **(b)**

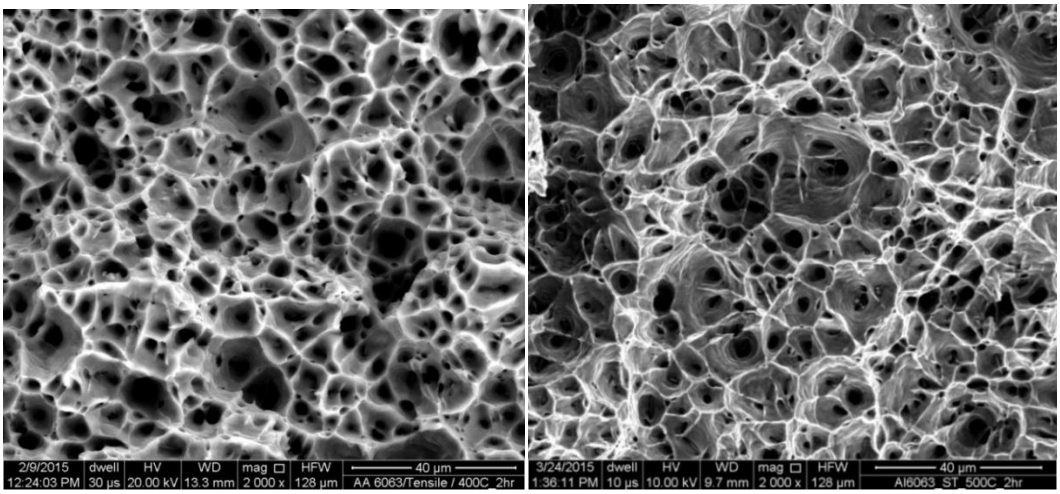

(c) **(d)**

Fig. 8.27 Honeycomb structure (dimples) on the surface of fractures of tensile specimens of AA6063 at :
(a) 300°C , (b) 350°C, (c) 400°C, (d) 500°C

8.4.3 AA6063 heat treated as 350℃ with different soaking time

Figure 8.28 shows the over view pictures after the LCF test for AA6063 heat treated at 350℃ with different soaking time.

Fracture surface of the fatigue tested samples was examined using scanning electron microscope (SEM). Ductile fracture was observed in all conditions, and at high heat treatment temperature of 350℃ with 8 hours of soaking time is observed to be ductility and deformations very high comparing with other conditions.

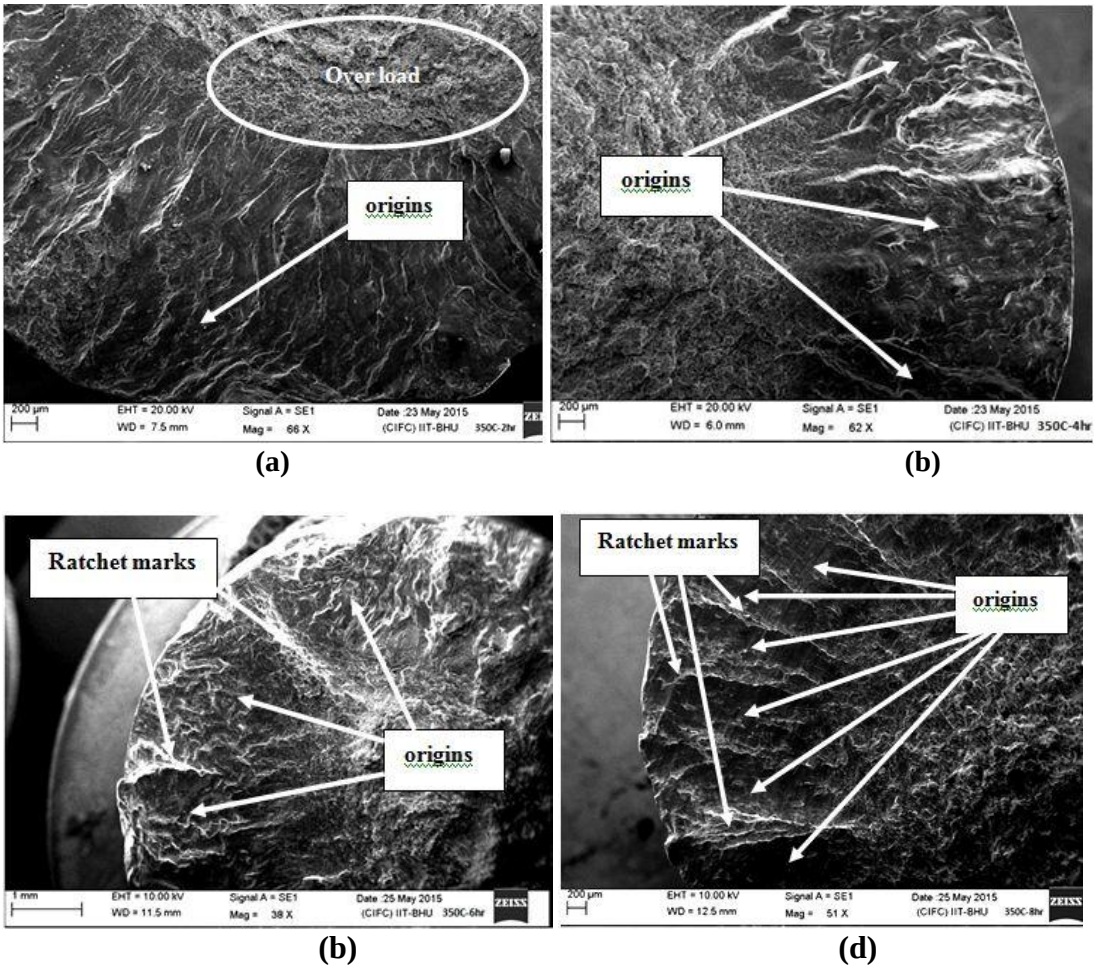

Fig. 8.28 SEM over view pictures after the LCF test for AA6063 treated at 350℃ with different soaking time:
(a) 2hours , (b) 4hours, (c) 6hours, (d) 8hours

It may be seen from these SEM pictures that dimple morphology was predominant at room temperature as well as at other elevated soaking time of heat treatment.

Figure 8.29 shows SEM pictures for AA6063 samples heat treated at different temperatures and at different soaking time. These pictures clearly show the direction of progression of fatigue crack which resemble to river on physical map.

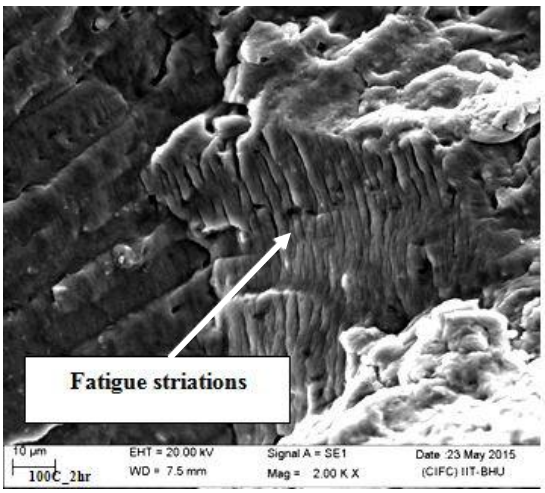

(a)

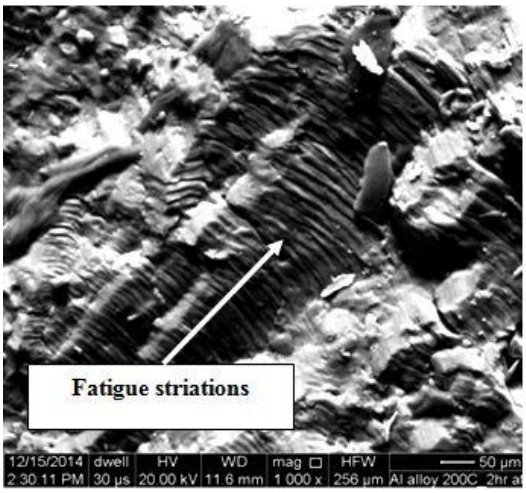

(b)

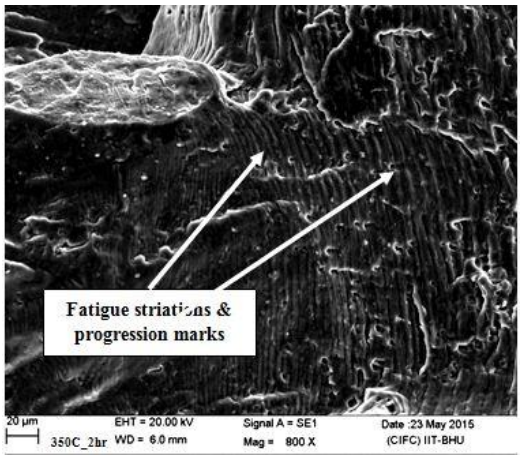

(c)

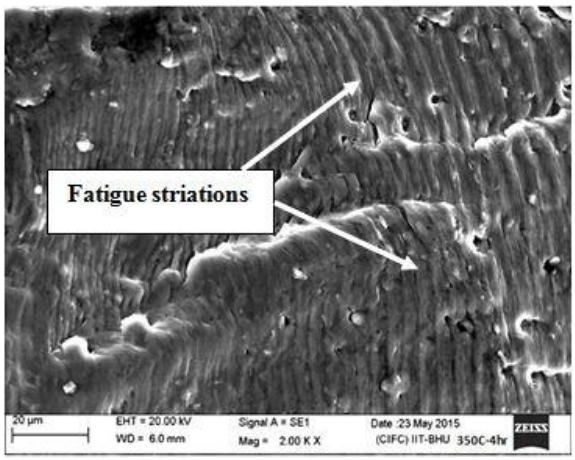

(d)

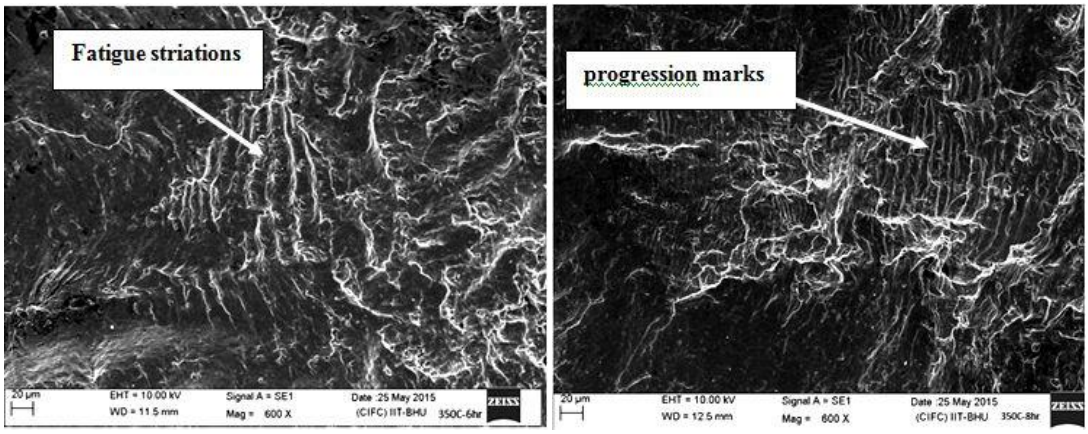

(e) **(f)**

Fig. 8.29 SEM Factograph (Segment) fracture surface of the Fatigue tested AA 6063 at different heat treatment conditions:
(a) 100°C_2hours, (b) 200°C_2hours, (c) 350°C_2hours, (d) 350°C_4hours
(e) 350°C_6hours, (f) 350°C_8hours

Plastic or ductile fracture is preceded by macroscopic plastic strain due to deformation in the slip planes as a result of higher fracture resistance in the cleavage planes and at grain boundaries. Plastic fracture is also called fibrous fracture because of its appearance or shear fracture because of the crack propagation mechanism.

In same time at high magnification we can see the Progression Marks (beach marks) , and these marks tell us exactly how the crack face has progressed across the test piece and are only present in fractures where there have been substantial variations in the component stress as the crack grew across the piece . Appearance of regular fatigue striations due to regular loading, still one striation per cycle can be observed in Fig. 8.29, and it is called ductile striations with large, regular size and spacing.

8.4.4 AA6063/SiCp MMC

The fracture surfaces of the specimens after fatigue testing were examined using scanning electron microscope. Fatigued specimens at different volume fraction were selected in order to study the characteristics of the fatigue crack formation and growth.

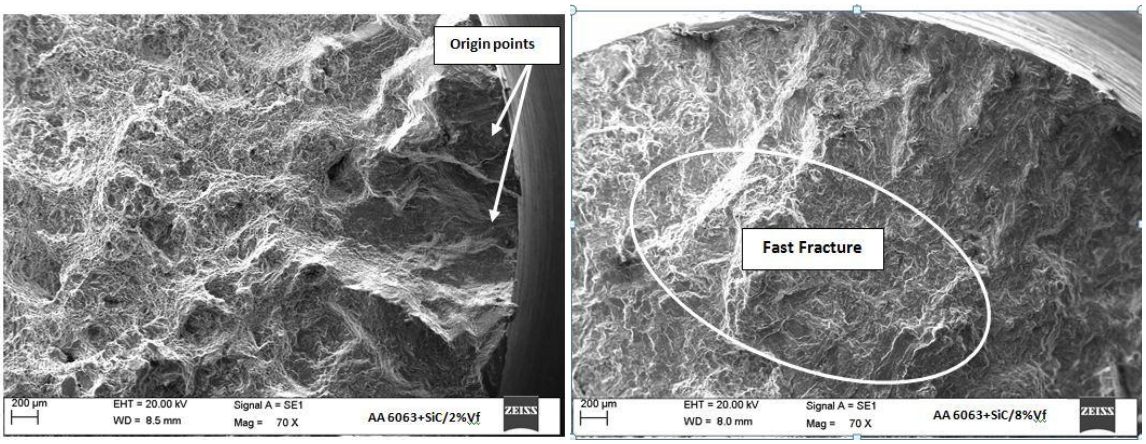

(a) **(b)**

Fig. 8. 30 SEM micrographs over view from the edge fracture surface of MMC AA6063/SiCp with (a) 2% V_f , (b) 8% V_f

All fracture surfaces had a dimple morphology, which indicates ductile fracture mode. Most of these dimples resulted from fracture or decohesion of SiC particles. There were mainly two dimple populations: the first one was related to SiC particles and increased in size as the size of the reinforcement particles were increased. The second population consisted of very small dimples located in the space between the reinforcement particles associated with fine intermetallic particles as observed in Fig. 8. 30. The particle cracking and cleavage between SiC and matrix material became more evident as the SiC size and content increased. There were a few observations of pull out of particles from the aluminium matrix, which indicates quite a good interfacial bonding as shown in Fig. 8. 30. High magnification SEM picture shows particle cracking and

cleavage between SiC particle and matrix material on fracture surface as shown in Fig. 8.31.

Two distinct fracture morphologies were observed: an initiation region and a fast fracture region. Higher magnifications of these two regions show that the fracture region around the initiation site did not have as many fractured or decohered particles as can be observed in Figs. 8.31(a, b) and the fast fracture region can be observed from Figs. 8.31(c, d) .

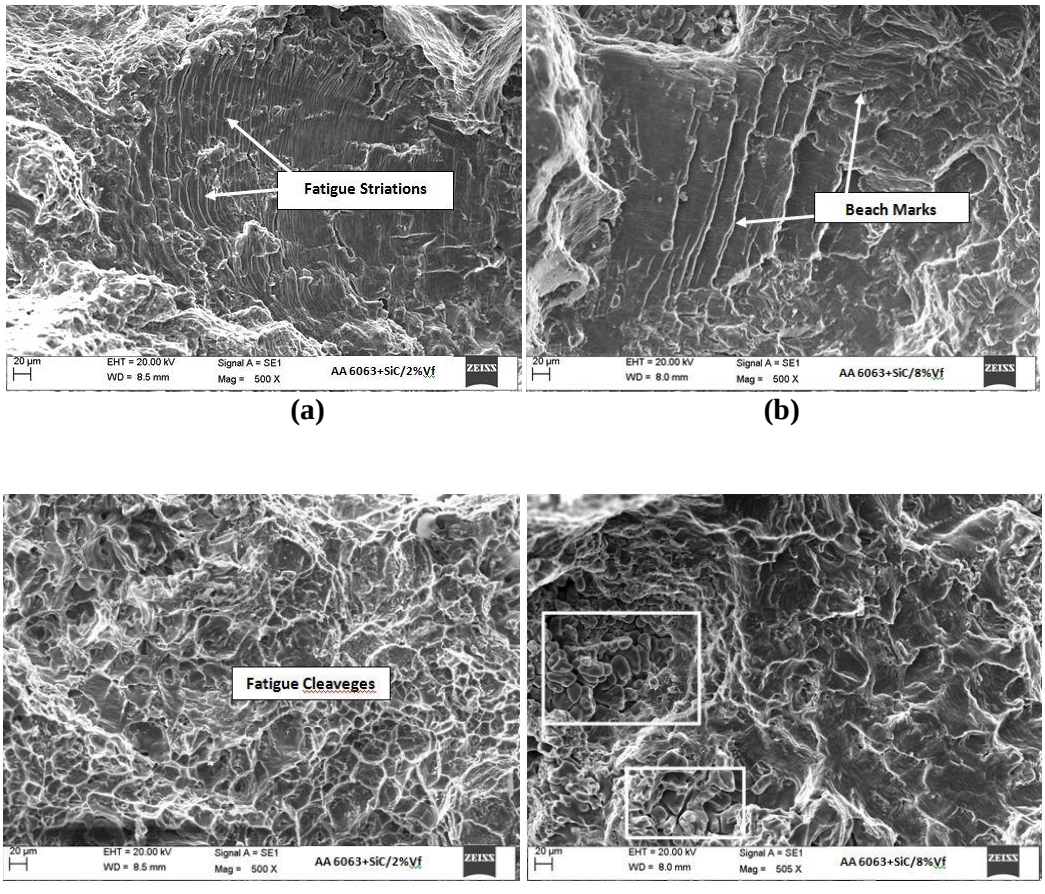

(a) **(b)**

(c) **(d)**

Fig. 8.31 SEM micrographs of MMC AA 6063/SiCp, (a) Fatigue striations at 2% V_f , (b) Beach marks of fatigue at 8% V_f, (c) fatigue initiation region at 2% V_f, (d) fast fracture region at 8% V_f.

8.4.5 Simply support beam

Electron microscopes are used in the study of fracture microstructure, in microfractography. Plastic or ductile fracture is preceded by macroscopic plastic strain due to deformation in the slip planes as a result of higher fracture resistance in the cleavage planes and at grain boundaries. Plastic fracture is also called fibrous fracture because of its appearance or shear fracture because of the crack propagation mechanism.

Dimples as a rule arise from microvoids, which exist in the material and grow during loading until they combine under plastic strain and plastic fracture. There were mainly two dimple populations: the first one was related to Si & Mg particles, the second population consisted of very small dimples located in the space between the reinforcement associated with the intermetallic particles.

A cross-sectional view of this fatigue failure shows that the piece is domed with the smallest radius near the outer edge. Also of interest is the shape of the overload zone. The fact that it is elongated indicates some plane bending loads were present, as demonstrated in Fig. 8.32. Micro cracks (initiating fracture) began almost simultaneously on parts of the circumference of the specimen. Here we can see the overload zone, or fast fracture zone, where the final catastrophic failure occurs.

The pictures of Fig. 8.33 look like a river on physical map, showing the direction of progression of the fatigue crack. And show up most frequently in the relatively fast-growing sections of the fatigue zone, and, other than indicating the direction of the crack growth**.**

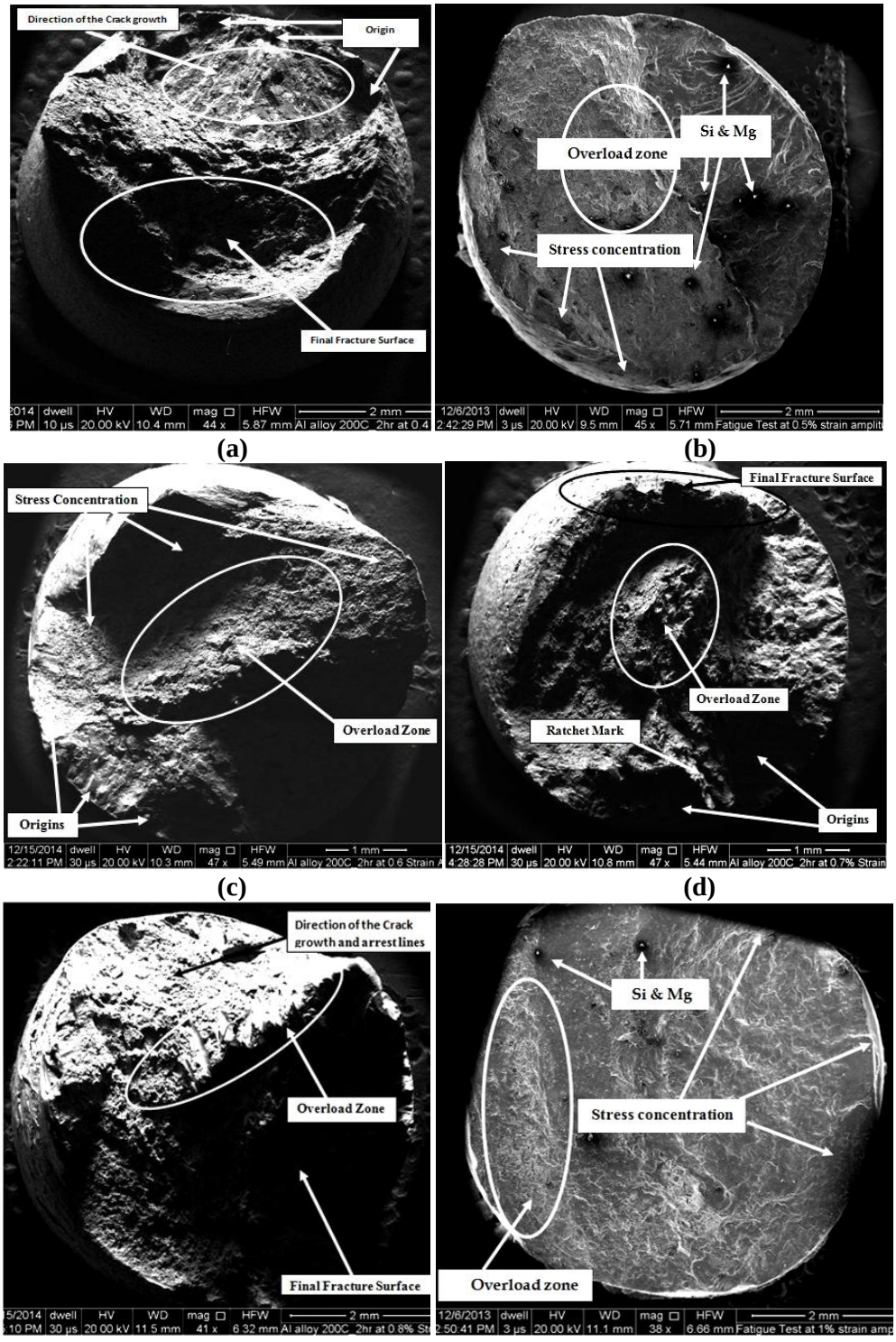

Fig. 8.32 SEM over view pictures for LCF simply supported samples at:

(a) 0.4% strain amplitude (b) 0.5% strain amplitude

(c) 0.6% strain amplitude (d) 0.7% strain amplitude

(e) 0.8% strain amplitude (f) 1% strain amplitude

This zone is usually macroscopically brittle, although in a small percentage ductility is present, and indicates the magnitude of the load when the final fracture occurs, that is, a large overload zone indicates the part was heavily stressed at the time of final fracture. The arrows as shown in Fig. 8.33(a) and Fig. 8.33(b) indicate the direction of the principal fatigue crack propagation.

Striations are the trace of a crack advancing in each cycle. They are perpendicular, or almost so, to the direction of crack propagation, although various exceptions have been noted. Striations may be continuous and regular, as in aluminum alloys, with the separation between them varying with the stress and the crack growth rate. They may also be discontinuous and irregular as illustrated in Fig. 8.33. In same time at high magnification we can see the Progression Marks (beach marks), and these marks tell us exactly how the crack face has progressed across the test piece. Figures 8.27(a) and Fig. 8.33 (b) show coarse and fine ductile dimples on the fracture surface of AA6063 material (strain amplitude = 0.5% and 0.4% R=-1, triangular wave).

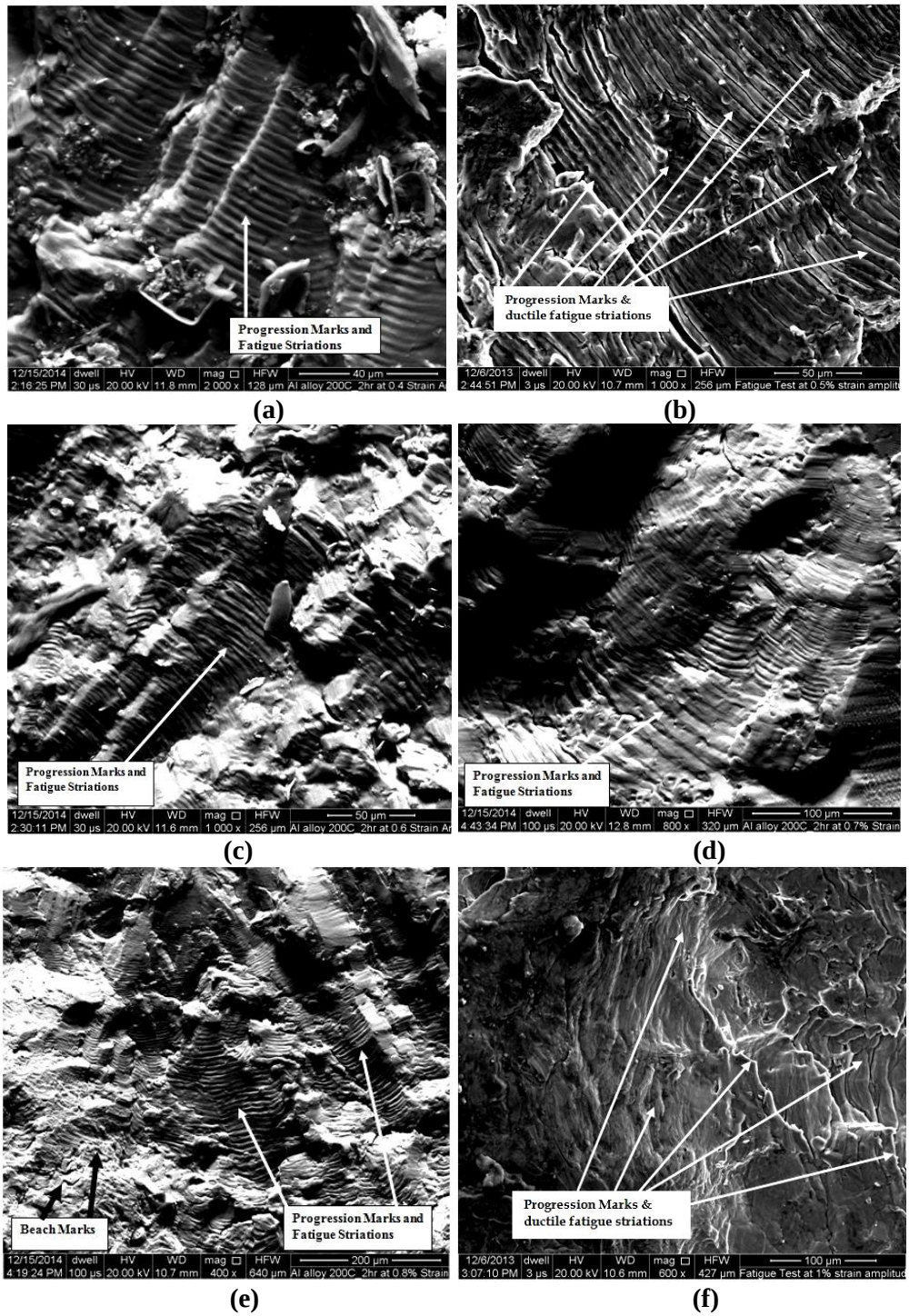

Fig. 8.33 Plastic Striations on a fracture of AA6063 as seen thorough a scanning electron microscope at different magnifications:

(a) 0.4% strain amplitude with 100µm (b) 0.5% strain amplitude with 40µm

(c) 0.6% strain amplitude with 100µm (d) 0.7% strain amplitude with 50µm

(e) 0.8% strain amplitude with 100µm (f) 1% strain amplitude with 200µm

8.9 Conclusion

Following major observations are made in this chapter.

1. Crystallite size and intensities of different crystal planes present in AA6063-T6 system are in agreement with the data available in JCPDF.
2. Crystallite size is observed to increase asymptotically with number of cycles to failure for as received AA6063-T6 alloy.
3. Diameter of samples at fracture decreases with increase in number of cycles of failure for as received AA6063-T6 alloy.
4. Crystallite size initially increases and after that decreases with heat treatment temperature for AA6063 alloy.
5. Diameter of sample at fracture decreases with increase in heat treatment temperature for AA6063 alloy while it increases with number of cycles of failure.
6. Soaking time of heat treatment at constant temperature has decreasing tendency with increase in soaking time.
7. Diameter at fracture initially decreases and after that increases with number of cycles of failure.
8. Crystallite size initially increases and afterwards decreases with increase in reinforcement particle volume fraction in MMC while diameter at fracture initially decreases and afterwards increases with increase in reinforcement particle volume fraction.
9. Diameter at fracture has a decreasing tendency with increase in number of cycles of failure.

10. Optical micrograph clearly shows slip-band dislocation and presence of crack for as received AA6063-T6 alloy.
11. Optical micrograph of MMC clearly shows presence of reinforcement particles.
12. SEM pictures show overload zone, progression marks, striation marks for as received AA6063-T6, heat treated at different temperature, heat treated at different soaking time, MMC, simply support samples. For cantilever specimen the elongated overload zone proves presence of bending load. Progression and fatigue striation marks show cyclic loading and direction of propagation of crack.